Biophysical Chemistry 24 (1986) 79–95
Elsevier

BPC 01057

ANALYSIS OF MULTI-COMPONENT FLUORESCENCE EMISSION BY PHASE-SENSITIVE DETECTION USING ONE MODULATION FREQUENCY

Susan M. KEATING-NAKAMOTO, Henryk CHEREK and Joseph R. LAKOWICZ *

Department of Biological Chemistry, University of Maryland, School of Medicine, 660 West Redwood Street, Baltimore, MD 21201, U.S.A.

Received 18th December 1985
Accepted 10th March 1986

Key words: Fluorescence lifetime; Phase-sensitive detection; Multi-component fluorescence emission

We describe the use of phase-sensitive detection of fluorescence to resolve the lifetimes and fractional intensities from multi-component fluorescence samples, using data obtained at a single modulation frequency. Phase-sensitive spectra of the mixture are recorded at arbitrarily chosen detector phase angles. The steady-state spectrum of each component must be known. The phase-sensitive spectra are fitted, using a nonlinear least-squares algorithm, to obtain the lifetimes and fractional intensities of each fluorophore in the mixture. Simulations for two- and three-component mixtures are presented to illustrate how the resolution is affected by spectral overlap and lifetime separation. Experimentally, we resolved two- and three-component mixtures of protein-like fluorophores (*N*-acetyl-L-tyrosinamide, *N*-acetyl-L-tryptophanamide, indole and 2,3-dimethylindole) using data collected at 30 MHz. These fluorophores have closely spaced lifetimes of 1.5, 2.9, 4.5 and 4.3 ns, respectively, and display extensive spectral overlap. These results demonstrate that phase-sensitive spectra, recorded at only one modulation frequency with a standard phase fluorometer, can be used to resolve multi-component emissions.

1. Introduction

A central difficulty of fluorescence spectroscopy is the resolution of multi-component emission. Such emission arises from both the intrinsic heterogeneity of single fluorophores and from the presence of multiple fluorophores. Many methods for the analysis of complex decays have been developed using both time-resolved [1–8] and phase-modulation spectroscopy [7–17]. The usual objective is to obtain the lifetimes and fractional intensities of the individual emitting species. At present, fixed-frequency phase fluorometers are widely available and permit measurement at two or three modulation frequencies. Using these instruments, two-component solutions have been resolved using an analytical solution [9–12], nonlinear least-squares [12–14] or phase-sensitive detection [15,16,18–21]. The analytical solution introduced by Weber [9], in which N lifetimes can be determined from phase and modulation data at N frequencies, has been used to resolve two-component solutions at two frequencies [10,12] or one frequency [11] using previously determined lifetimes. Fitting methods have also been used to determine the lifetimes of two components using data from two or three frequencies [12–14]. Phase-sensitive detection has been used to recover the lifetimes or emission spectra by adjustment of the detector phase angle to be out of phase with the emission of one of the components [16,18]. In general, all the above methods are rather cumbersome, requiring either precision in excess of that

* To whom correspondence should be addressed.

Abbreviations: DMI, 2,3-dimethylindole; NATrA, *N*-acetyl-L-tryptophanamide; NATyA, *N*-acetyl-L-tyrosinamide; p-ter, *p*-terphenyl; POPOP, *p*-bis[2-(5-phenyloxazolyl)]benzene; 9-MA, 9-methylanthracene; 9,10-DPA, 9,10-diphenylanthracene; PSD, phase-sensitive detection; ϕ_D, detector phase angle.

generally available or careful adjustment of the detector phase angles.

We developed a simpler method for the resolution of multi-component emission using phase-sensitive detection. Phase-sensitive spectra are recorded at a number of arbitrarily chosen detector phase angles. The steady-state emission spectra of the suspected components in the mixture are recorded separately. A nonlinear least-squares algorithm fits the measured phase-sensitive spectra to calculated values, yielding the lifetimes and fractional intensities of the individual components. In a preliminary report we used this method to resolve successfully mixtures of POPOP, 9-MA and 9,10-DPA [22]. We now describe this procedure more completely. Simulated data for two- and three-component solutions are used to illustrate the appearance of the data, and how the resolution of lifetimes and fractional intensities is affected by increasing spectral overlap and decreasing lifetime separation. Additionally, we present the experimental resolution of two- and three-component mixtures of tryptophan and tyrosine derivatives, with extensive spectral overlap and closely spaced lifetimes of 1.5, 2.9, 4.5 and 4.3 ns.

Our method for the analysis of phase-sensitive spectra allows for the first time the resolution of three-component mixtures from data collected with one modulation frequency, without previous knowledge of the lifetimes or fractional intensities. Another advantage of this technique is relatively rapid data acquisition. A disadvantage of the technique is the requirement for known steady-state spectra.

2. Theory

In phase-modulation fluorometry the sample is excited with modulated light described by,

$$I(t) = 1 + m_{ex} \sin \omega t \tag{1}$$

where $\omega = 2\pi F$ is the circular modulation frequency, F the frequency in cycles/s and m_{ex} the modulation of the exciting light. The emission is also modulated but delayed by a phase angle ϕ and demodulated by a factor m, relative to the exciting light,

$$F(t) = 1 + m_{ex} m_1 \sin(\omega t - \phi_1) \tag{2}$$

For a single-exponential decay the lifetime (τ_1) can be calculated from the measured quantities ϕ_1 and m_1 using

$$\tan \phi_1 = \omega \tau_1 \tag{3}$$

$$m_1 = \left(1 + \omega^2 \tau_1^2\right)^{-1/2} \tag{4}$$

If the fluorescence is due to more than one species the individual lifetimes (τ_i) must be determined by other methods [8].

For multi-component samples the modulated emission is a sum of the modulated intensity of each component,

$$F(t) = \sum_i k_i m_i \sin(\omega t - \phi_i) \tag{5}$$

where k is a constant which depends upon the emission wavelength, concentration, extinction coefficient and quantum yield of each component. For each single-exponential component in the decay $m_i = \cos \phi_i$.

In phase-sensitive detection, the wavelength-dependent emission is scanned as usual, but recorded with a phase-sensitive detector [16]. The phase-sensitive spectrum $I_p(\lambda, \phi_D)$ is proportional to the steady-state intensity of each component and the cosine of the phase difference between the emission of each component and the detector phase angle;

$$I_p(\lambda, \phi_D) = k \sum_i f_i m_i I_i(\lambda) \cos(\phi_D - \phi_i) \tag{6}$$

Here, λ is the emission wavelength, ϕ_D the detector phase angle relative the incident light and k a constant. For the i-th component f_i is the steady-state fractional intensity, $\Sigma_i f_i = 1.0$, and $I_i(\lambda)$ the area-normalized steady-state spectrum $\Sigma_\lambda I_i(\lambda) = 1.0$. The phase-sensitive signal of each component is proportional to the cosine of the difference between the detector phase angle and the phase angle of that component as $\cos(\phi_D - \phi_i)$. For many fluorophores the lifetime, or phase angle, is constant across the emission spectrum. As ϕ_D is varied the contribution of each component to the phase-sensitive spectra also varies. Because the

observed phase-sensitive intensity is a sum of the individual phase-sensitive intensities, the total intensity and spectral shape vary with ϕ_D. This variation of the phase-sensitive spectra with ϕ_D is the basis for calculating the individual lifetimes and fractional intensities from the spectra.

We recover the lifetimes and fractional intensities by the procedure of nonlinear least squares, based on the Marquardt algorithm as described by Bevington (chapter 11 in ref. 31). We simultaneously measure two phase-sensitive spectra, one at the detector phase angle, ϕ_D and the other at $\phi_D + 90°$. We arbitrarily refer to these as the in-phase, I_p, and quadrature, I_q, signals. Both sets of spectra are fitted in an iterative manner to calculated phase-sensitive spectra:

$$I_{cp}(\lambda, \phi_D) = \sum_i f_{ci} \cos \phi_{ci} I_i(\lambda) \cos(\phi_D - \phi_{ci}) \tag{7}$$

$$I_{cq}(\lambda, \phi_D) = \sum_i f_{ci} \cos \phi_{ci} I_i(\lambda) \times \cos(\phi_D + 90° - \phi_{ci}) \tag{8}$$

In these equations the assumed or calculated parameters are identified by the subscript c. The fractional intensities (f_{ci}) and the individual phase angles (ϕ_{ci}) are varied to obtain the best match between the measured (I_p and I_q) and calculated (I_{cp} and I_{cp}) spectra. The match is determined by searching for the minimum value of χ^2, which is the error-weighted sum of the squared deviations between the measured and calculated data,

$$\chi^2 = \sum_{\phi_D} \sum_{\lambda} 1/\sigma^2 \left[I_p(\lambda, \phi_D) - I_{cp}(\lambda, \phi_D) + I_q(\lambda, \phi_D) - I_{cq}(\lambda, \phi_D) \right]^2 \tag{9}$$

The weighting factor (σ) will be discussed below. The values of ϕ_{ci} and f_{ci} are those which minimize χ^2. The ϕ_{ci} are used to calculate the lifetimes by eq. 3. The goodness of fit is judged by the value of the reduced χ^2,

$$\chi^2_R = \chi^2/\nu \tag{10}$$

where ν is the number of degrees of freedom,

$$\nu = 2N_\lambda N_D - p. \tag{11}$$

in which N_λ is the number of emission wavelengths, N_D the number of detector phase angles and p the number of floating parameters (one for the first component, and two for each additional component). For values of ϕ_{ci} and f_{ci} which adequately describe the sample, the value of χ^2_R is expected to fluctuate near 1.0, assuming the data contain random experimental errors.

The magnitude of χ^2_R is dependent on the weighting factor used. The usual weighting factor for a nonlinear least-squares analysis is $1/\sigma^2$, where $(\sigma^2)^{1/2}$ is the standard deviation of the measurement [31]. In our measurements the noise level is probably statistical and dependent on the total signal level (photons/time interval) [32]. The standard deviation of such signals is often estimated by the square root of the total signal level [31,32]. The total signal should be considered, and not the phase-sensitive intensity, because the noise exists independently of the phase-sensitive detector and its phase angle. Hence, the noise in the phase-sensitive intensity should be comparable to that in the total fluorescence intensity. However, it was not convenient to measure the total signal level simultaneously with the phase-sensitive spectra. This is because the two signals should be measured using the same gain, which was not practical since our lock-in amplifier does not amplify the d.c. component of the modulated signal. However, the total amplitude of the modulated emission or magnitude spectra, $I_m(\lambda)$, was available as a direct output of the lock-in amplifier. We measured this signal simultaneously and at the same gain as the phase-sensitive spectra. The magnitude spectrum is proportional to the total steady-state spectra after attenuation of each component by m_i;

$$I_m(\lambda) = k \sum_i f_i m_i I_i(\lambda) \tag{12}$$

The average value of $I_m(\lambda)$ over the measured wavelengths $\overline{I_m(\lambda)}$, was used in the weighting factor

$$\sigma = 0.01 S \left(\overline{I_m(\lambda)}\right)^{1/2} \tag{13}$$

where S is the percentage noise estimated for the data.

3. Methods

3.1. Measurements

The data were obtained using a phase-modulation spectrofluorometer with a 30 MHz modulation frequency, 280 nm excitation, an excitation bandpass of 4 nm, an emission bandpass of 16 nm and the polarizers removed for increased sensitivity. The transmission properties of the emission monochrometer distort the emission spectra between 380 and 410 nm. This artifact could be eliminated by use of a polarizer. However, this was unacceptable due to the decreased intensity and signal-to-noise ratio. The emission wavelengths varied from 290 to 450 nm, at 5-nm steps and 5 s per step. Data collected at 5-nm intervals gave similar results to those collected at 1-nm steps, but the use of 5-nm intervals substantially decreased the time needed for acquisition and analysis. Steady-state spectra of single-component solutions were measured in the same instrument with unmodulated illumination. For phase-sensitive spectra the cross-correlated signal from the phase fluorometer was measured with a model 5204 lock-in analyzer (Princeton Applied Research) using 250 mV sensitivity and a 0.1 Hz time constant.

It is necessary to know the value of the detector phase angles, ϕ_D, relative to the phase angle of the modulated excitation, and to minimize the dependence of the time response of the photomultiplier on the wavelength and geometrical distribution of light incident upon the photocathode [33]. The phase angle of a reference fluorophore, ϕ_{ref}, was determined before each scan [16] and the apparent value used to determine the actual value of ϕ_D. In this study p-ter was used with a reference lifetime of 1.05 ns. The phase shift of p-ter is 11.17° at 30 MHz (eq. 3). The phase shift of a fluorophore corresponds to the value of the detector phase angle at which its phase-sensitive intensity is at a maximum. In practice, it is more precise to determine the phase angle of a fluorophore by finding the detector phase angle that gives complete suppression of the signal, at $\phi_D + 90°$ [16]. The true phase angle ϕ_D is obtained by adding $\phi_{ref} = 11.17°$ to the apparent phase angle.

The detector phase angle was set to the desired value and the phase-sensitive spectra were obtained by scanning the emission wavelength. Typically 8–20 phase-sensitive spectra were recorded at arbitrarily chosen detector phase angles between 0 and 280°. Initially, spectra at about 20 different ϕ_D were recorded, but it was noticed that slightly better results were obtained using fewer spectra. This was probably due to the shorter time for data acquisition and instability of the degree of modulation of the exciting light over long periods of time. The spectra were recorded using data acquisition programs for a MINC 11/23 computer (Digital Equipment Corp.). The program samples 20 intensities per wavelength at a rate of 20 per s, after a stabilization period following each change in wavelength. The computer simultaneously records the in-phase (ϕ_D), quadrature ($\phi_D + 90°$) and magnitude spectra.

Indole, DMI, NATyA, NATrA and p-ter were obtained from Aldrich Chemical Co. and used without further purification. All solutions were measured at 20°C, in 25 mM Tris-HCl (pH 7.5) except p-ter was in 100% ethanol. The lifetimes of the individual components were measured as described previously [30,33], relative to p-ter with the excitation and emission polarizers removed and the emission observed using 10 nm bandpass interference filters. These filters were NATyA, 313 nm; NATrA, 360 nm; Indole, 340 nm; and DMI, 380 nm. The lifetimes shown are the average of the phase and modulation lifetimes which are approximately equal in all cases.

3.2. Analysis

The phase-sensitive spectra were fitted using one to four components, where the number of components represents the number of emission spectra and lifetimes used by the fitting algorithm. Generally the fractional intensities and the lifetimes are all variables in the analysis, but our program allows any individual parameter to be held constant. The absolute magnitude of χ^2_R depends on the percentage noise (S) assumed to be present in the data. This value is chosen by experience. For instance, if analysis of a known two-component mixture with a two-component model

yields χ^2_R near unity with 3% noise, then one knows the actual noise level is near 3%. Selection of the correct number of components is in no way limited by the value of S. The chosen value of S does not alter the relative values of χ^2_R for different numbers of components. The use of a percentage noise is conceptually convenient in that we maintain some estimate of the quality of the data, and the χ^2_R values are easily interpreted.

Our analysis program, written in Basic-11, runs on both MINC 11/23 and DEC 11/73 computers and may be obtained from J.R.L. This program uses analytical derivatives with respect to f_i and ϕ_i

$$\frac{\partial I_p(\lambda, \phi_D)_i}{\partial \phi_i} = f_i \cos \phi_1 I_i(\lambda) \sin(\phi_D - \phi_i) - f_i \sin \phi_i I_i(\lambda) \cos(\phi_D - \phi_i) \quad (14)$$

$$\frac{\partial I_p(\lambda, \phi_D)_i}{\partial f_i} = \cos \phi_i I_i(\lambda) \cos(\phi_D - \phi_i) \quad (15)$$

3.3. Simulations

For simulations the steady-state spectra were modeled by Gaussian distributions,

$$I_{si}(\lambda) = \frac{100}{w_i\sqrt{2\pi}} \exp\left[-\frac{1}{2}\left(\frac{\lambda - \bar{\lambda}_i}{w_i}\right)^2\right] \quad (16)$$

where $\bar{\lambda}_i$ is the emission maximum of the i-th component and w_i the 'standard deviation' of the spectral distribution. This parameter is related to the full-width at half-maximum (Γ_i) by $\Gamma_i = 2.354 w_i$. Phase-sensitive spectra with random noise were simulated using eqs. 7, 8 and 12. Typically, data were simulated from 300 to 450 nm at 5-nm steps, for 10 detector phase angles between 20 and 200° of in-phase data and 110 and 290° for quadrature data (10 files with 20 ϕ_D). For all simulations the full-width at half-maximum equalled 50 nm, the modulation frequency was 30 MHz, $f_1 = f_2 = 0.5$ for two-component data and $f_1 = f_2 = f_3 = 0.33$ for three-component data. The simulated data were analyzed exactly as the experimental data. In some cases an incorrect steady-state spectrum was used in the analysis, or one of the component lifetimes was held constant at an incorrect value.

4. Results

4.1. Simulated phase-sensitive spectra

Simulated phase-sensitive spectra for two- and three-component solutions are shown to illustrate the appearance of the data. A two-component example is shown in fig. 1. The top panel shows the steady-state spectra for each of the two components; one with an emission maximum of ($\bar{\lambda}_1$) 330 nm (———) and the second with an emission maximum ($\bar{\lambda}_2$) of 380 nm (— — —). The magni-

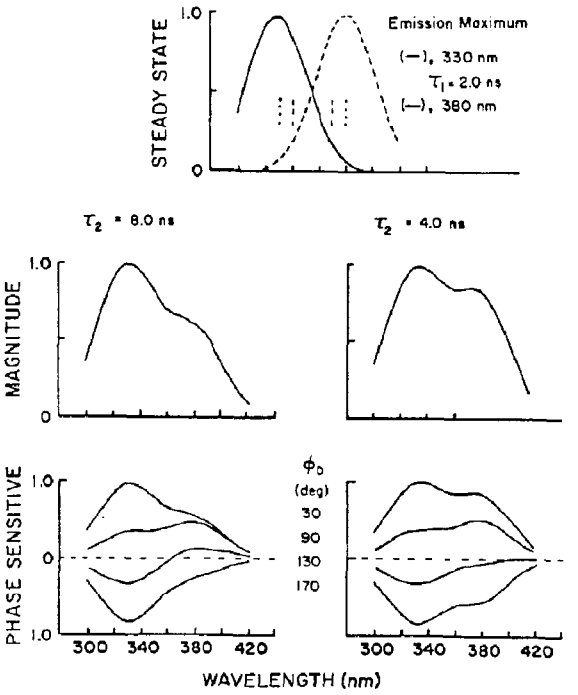

Fig. 1. Two-component simulated data. (Top) Steady-state emission spectra of two components; component 1 with an emission maximum, $\bar{\lambda}_1 = 330$ nm, $\tau_1 = 2$ ns (———) and component 2 with an emission maximum $\bar{\lambda}_2 = 380$ nm (— — —). (Middle) Magnitude spectrum for the mixture with $\tau_2 = 8$ ns (left) or 4 ns (right). (Bottom) Phase-sensitive spectra of the mixtures at $\phi_D = 30$, 90, 130 and 170°.

tude spectrum shown in the middle left panel is for $\tau_1 = 2$ ns and $\tau_2 = 8$ ns. The modulated intensity of the second 380 nm component is lower than that of the 330 nm component because the 8.0 ns lifetime results in more demodulation than the 2.0 ns lifetime. At 30 MHz a 2.0 ns lifetime has a demodulation factor (m) of 0.936 while for 8.0 ns $m = 0.556$ (eq. 4). The magnitude spectrum is the sum of the steady-state spectrum of each component attenuated by the fractional intensity and demodulation factor of that component (eq. 12).

Representative phase-sensitive spectra of this simulated mixture are shown at the bottom left in fig. 1 for $\phi_D = 30$, 90, 130 and 170°. At 30° the phase-sensitive intensity of the first component is larger than that of the second component. As the value of the ϕ_D is increased to 90°, the phase-sensitive intensity of component 1 decreases more rapidly than that of component 2. At 130° the phase-sensitive intensity of component 1 is negative while that of component 2 is still positive. Finally, as ϕ_D increases to 170° the phase-sensitive intensities of both components become negative. This variation is due to the dependence of the phase-sensitive intensity of each component on ϕ_D and ϕ_i. As the value of ϕ_D increases, $\cos(\phi_D - \phi_1)$ decreases more rapidly than $\cos(\phi_D - \phi_2)$ when ϕ_1 is smaller than ϕ_2. For example, here $\phi_1 = 21°$ and $\phi_2 = 56°$ at 30 MHz (eq. 3). This figure demonstrates that the phase-sensitive intensity of the sample is a sum of the phase-sensitive intensities of each component. Importantly, the phase-sensitive intensity of each component varies with changes in ϕ_D. This differential weighting of the individual contributions to the phase-sensitive spectra forms the basis for resolving the individual components.

For comparison the right-hand side of fig. 1 illustrates the corresponding spectra for a solution with identical spectra except that $\tau_2 = 4.0$ rather than 8.0 ns. The shorter second lifetime results in a different shape of the magnitude spectrum due to less demodulation of the 4 ns lifetime ($m = 0.799$) relative to a 2.0 ns lifetime ($m = 0.936$). The phase-sensitive spectra of the solution with $\tau_2 = 4.0$ ns (lower right) are distinct from those with $\tau_2 = 8$ ns (lower right) at the same ϕ_D. The dependence of the phase-sensitive spectra on the component lifetimes (or ϕ_i) and detector phase angles (ϕ_D) permit the resolution of the lifetimes and fractional intensities for mixtures of fluorophores.

Simulations for a three-component mixture are shown in fig. 2 The top panel shows the steady-state spectrum of each component. The emission maxima of the first and second components are as in fig. 1 and a third component is added with an emission maximum of 430 nm (●). The middle of the figure shows the magnitude spectrum if $\tau_1 = 2.0$ ns, $\tau_2 = 5.0$ ns and $\tau_3 = 8.0$ ns (left) or 3.5 ns (right). The three Gaussian shapes are discernable in the spectra. As the lifetimes increase from 2.0 to 8.0 ns, the magnitude spectrum of each component is less intense. The bottom panels show the phase-sensitive spectra at the same detector phase angles as in fig. 1. As for the two-component data,

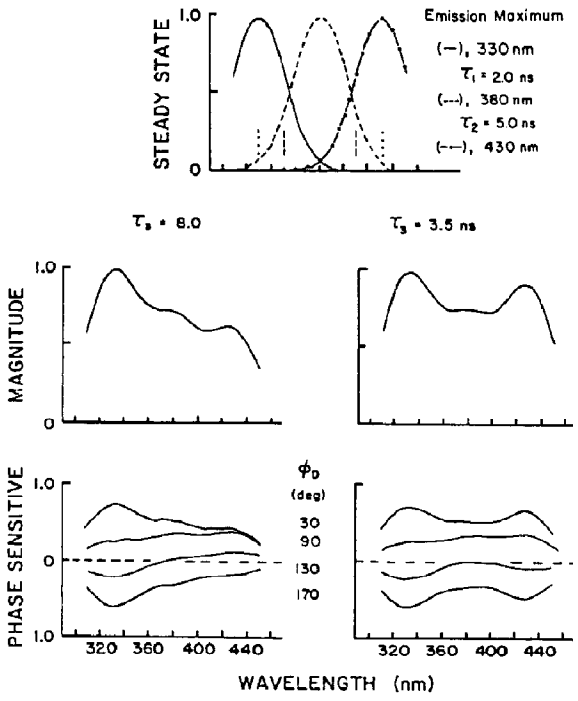

Fig. 2. Three-component simulated data. (Top) Steady-state emission spectra of each component; $\bar{\lambda}_1 = 330$ nm, $\tau_1 = 2$ ns (———); $\bar{\lambda}_2 = 380$ nm, $\tau_2 = 5$ ns (— — —); $\bar{\lambda}_3 = 430$ nm (●———●). (Middle) Magnitude spectra for $\tau_3 = 8$ ns (left) or 3.5 ns (right). (Bottom) Phase-sensitive spectra at $\phi_D = 30$, 90, 130 and 170°.

the relative phase-sensitive intensities of each component vary with the value of ϕ_D, resulting in different spectral shapes. The right-hand side of fig. 2 illustrates the magnitude and phase-sensitive spectra for a three-component solution where all components are identical to those shown on the left, except that $\tau_3 = 3.5$ ns. The reduction of the third component lifetime from 8.0 to 3.5 ns results in an increased intensity of that component in the magnitude spectrum and phase-sensitive spectra at 430 nm, due to the higher modulation of component 3. Clearly, the addition of a third component to the simulated data introduces a more difficult resolution than two-component data.

The phase-sensitive spectra depend on the spectral separation of the components (fig. 3). In this case the third component was positioned between the 330 and 380 emission maxima of the first two components. The spectral separation is thus decreased from 50 to 25 nm, as shown at the top of the figure. For this set of simulated data $\tau_1 = 2.0$, $\tau_2 = 5.0$ and $\tau_3 = 8.0$ ns. The dependence of the phase-sensitive spectra on the spectral distribution of the components is illustrated by comparison of the phase-sensitive spectra of the two different sets of data at the same ϕ_D (figs. 2 and 3). The third component at 355 nm results in less obvious contributions of each component to the spectra. Figs. 1–3 reveal the overall dependence of the shape of the sample phase-sensitive spectra on the lifetimes and the emission maxima of the individual components. We now question whether the least-squares analysis of phase-sensitive spectra can yield reliable resolution of the individual components.

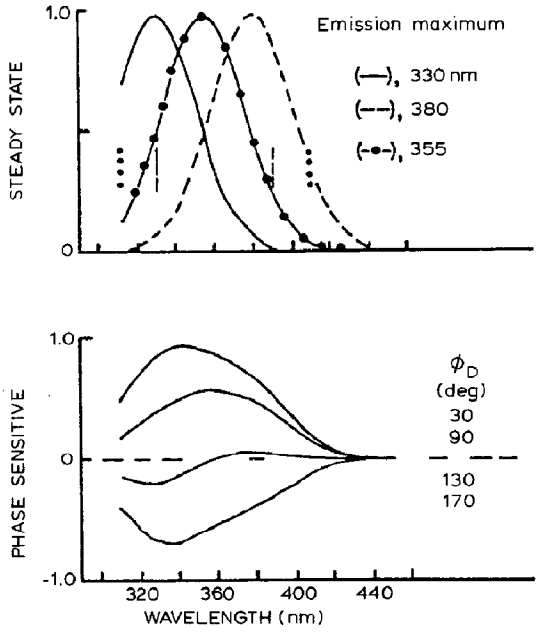

Fig. 3. Three-component simulated data. (Top) Steady-state emission spectra as shown in fig. 2 except that the emission maximum of component 3 is 355 nm (●———●). (Bottom) Phase-sensitive spectra for ϕ_D = 30, 90, 130 and 170°.

4.2. *Analysis of simulated data*

Simulated data with random noise were analyzed just as experimental data to determine the individual spectra and lifetimes. The dependence of χ^2_R on these parameters should indicate the reliability of the values recovered from the analysis, and how the uncertainties change as the lifetimes and spectra are brought closer together [17,31]. The results from the analysis of the two-component simulation in fig. 1 are shown in fig. 4. The solid lines are for fits of the widely spaced lifetimes ($\tau_1 = 2$ ns and $\tau_2 = 8$ ns) and the dashed lines for $\tau_1 = 2$ ns and $\tau_2 = 4$ ns. Although the data were simulated between 300 and 420 nm at 5-nm intervals, the data were fit using 11 wavelengths between 330 and 380 nm, as shown by the two vertical dotted lines in fig. 1. Also, a total of 20 phase-sensitive spectra were analyzed (10 in-phase and 10 quadrature spectra). To determine the dependence of χ^2_R upon the parameter values either τ_1 or τ_2 was held constant at a value different from the correct one. If the value of χ^2_R changes by only a small amount when a parameter is held constant this different value cannot be reasonably distinguished from the true value. Conversely, if the values of χ^2_R increase dramatically one may conclude that the value of the parameter can be rejected. Alternatively, the steepness of the parabolas can be viewed as revealing the available resolution. Steep parabolas have well defined minima, and hence the parameter values are well defined. Conversely, if the parabolas show broad

minima then χ^2_R does not vary greatly for values of the parameters near the minima. In fig. 4 (top) the solid line parabola centered at 2 ns represents the values of χ^2_R that were a result of holding τ_1 constant and the parabola centered at 8 ns shows the values of χ^2_R that occurred when τ_2 was held constant. When $\tau_1 = 2.0$ ns then $\chi^2_R = 1.0$. If τ_1 was held at 1.5 or 2.5 ns, the value of χ^2_R increased 70-fold, indicating that the value of τ_1 can be accurately determined. When τ_2 was held constant at 7.5 and 8.5 ns the value of χ^2_R increased to 4, and to larger values as the value of τ_2 was varied further. Although a 4-fold increase in χ^2_R is not as dramatic as the 70-fold increase of the 2.0 ns component, it is large enough to determine τ_2 accurately. If the number of degrees of freedom $\nu = 200$ it is only 0.1% probable that a set of data

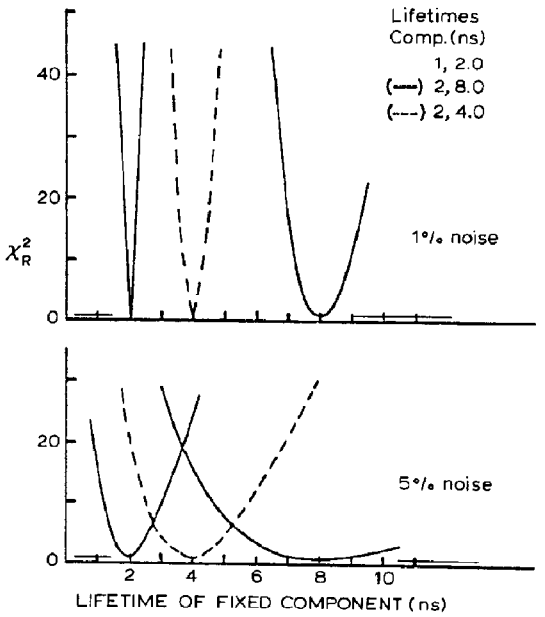

Fig. 4. The dependence of χ^2_R on the lifetimes of a two-component mixture. The parameters are those used in fig. 1: $\bar{\lambda}_1 = 330$ nm, $\bar{\lambda}_2 = 380$ nm, $\tau_1 = 2$ ns (———) and $\tau_2 = 8$ (———) or 4 ns (— — —). The random noise was 1% (top) or 5% (bottom). The simulated data were analyzed holding one lifetime constant at the value shown on the abscissa. The other lifetimes and fractional intensities were allowed to float. The correct component steady-state spectra were used. Ten simulated data sets consisted of 10 ϕ_D between 20 and 200° of in-phase data and 10 ϕ_D between 110 and 290° of quadrature data.

with random experimental error would yield $\chi^2_R = 1.34$, compared to another fit with $\chi^2_R = 1.0$. Here, for 11 wavelengths, 10 ϕ_D and two components, $\nu = 217$. The probability that statistical variation would give a 4-fold increase in χ^2_R is too low to accept the lifetime values yielding the higher value of χ^2_R. It should be noted that the less dramatic dependence of χ^2_R on τ_2 is probably due to the smaller modulated amplitude of the 8.0 ns component relative to the 2.0 ns component. The smaller spectral contribution translates into a smaller difference between the simulated and calculated values for the incorrect lifetime. Since the increase in χ^2_R is not as great, the resolution of the second lifetime is less precise.

Similar fits were performed for the simulated data with $\tau_2 = 4.0$ ns. The values of χ^2_R that result from holding τ_2 constant are shown as dashed lines (fig. 4). When τ_2 is held constant at values ± 0.5 ns from 4.0 ns, χ^2_R increases about 18-fold. When τ_1 is varied, the increase in χ^2_R is similar to that seen when $\tau_2 = 8.0$ ns (about 50-fold). (These results are nearly superimposable on the solid parabola at 2 ns when $\tau_2 = 8$ ns.) Surprisingly, the reduced separation of the lifetimes does not reduce the precision of the two-lifetime resolution. In fact, the resolution of $\tau_2 = 4$ ns appears to be more precise than for $\tau_2 = 8$ ns. Again, the larger changes in χ^2_R when τ_2 has a smaller value are probably due to the increased modulation of the 4.0 ns signal compared to that of the 8.0 ns component. The ability to resolve the lifetimes depends on the demodulation factor of each component. Components with long lifetimes will be strongly demodulated, and the lifetimes will not be accurately determined by these procedures.

We also investigated the dependence of χ^2_R on the emission maxima of the components. This sensitivity was determined by introducing an incorrect steady-state spectrum for one component with the correct spectrum for the other. The data were fitted using both lifetimes and fractional intensities as floating parameters. This analysis illustrates the ability to discriminate between the correct and incorrect emission spectra. Analysis of data with $\tau_1 = 2.0$ and $\tau_2 = 8.0$ ns, $\bar{\lambda}_1 = 330$ nm and $\bar{\lambda}_2 = 380$ nm, is shown in fig. 5. The parabola centered at 330 nm (———) illustrates the values

of χ^2_R when the steady-state spectrum for component 1 was shifted from the correct emission maximum of 330 nm. The parabola (———) centered at 380 nm illustrates the effect of shifting the second emission maximum. Clearly, χ^2_R is very dependent on the steady-state spectra; χ^2_R increases 75-fold when the first component spectrum is shifted 5 nm, and 25-fold when the second component spectrum is shifted 5 nm. The dashed lines centered at 380 nm are the values of χ^2_R when $\tau_2 = 4$ ns. The two parabolas ($\tau_2 = 4$ or 8 ns) centered at 330 nm are superimposable. It is apparent that decreasing the lifetime separation from 4- to 2-fold does not decrease the spectral resolution. In fact, when the second spectrum with $\tau_2 = 4$ ns is shifted 5 nm, χ^2_R increases 33-fold. The larger values of χ^2_R for $\tau_2 = 4.0$ rather than 8.0 ns are due to the larger modulated amplitude of the 4 ns component.

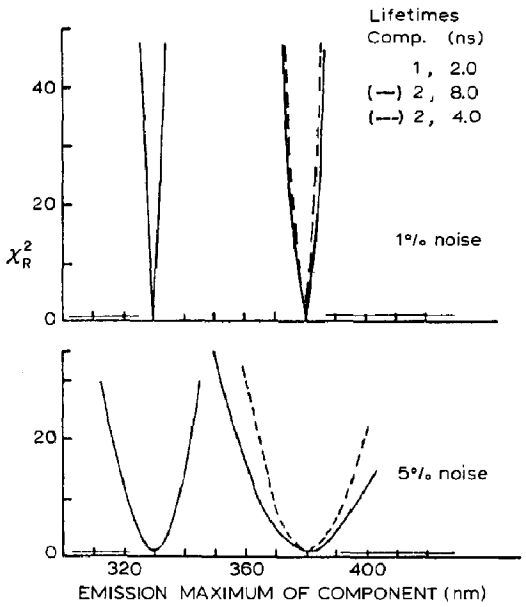

Fig. 5. The dependence of χ^2_R on the emission maxima of simulated two-component mixtures. The data from fig. 4, with $\tau_1 = 2$ ns (———) and $\tau_2 = 8$ (———) or 4 (— — —) ns, were fitted using one incorrect emission maximum, as indicated on the abscissa. The lifetimes and fractional intensities were allowed to float.

In all cases the simulated data contained 1–5% random noise. For experimental data the noise level appears to be near 3%. The top portions of figs. 4 and 5 show the results of analysis of data with 1% noise and the bottom 5% noise. As expected, as the amount of noise in the simulated data is increased, the changes in χ^2_R are not as great as observed at lower noise levels. Thus, the precision of the resolution decreases as the noise increases. For example, the precision in the resolution of the 8.0 ns lifetime (bottom, fig. 4) is low. The values of χ^2_R are about 1.5 when the value of τ_2 is held constant at 7 or 9 ns, while at 1% noise, χ^2_R is near 13 for these lifetime values. We also examined data with more closely spaced emission spectra. For brevity, these results are not shown in detail. However, decreasing the spectral separation of the two components from 50 to 30 nm had only a modest effect on the resolution.

At this point it seems valuable to explain our approach to analyzing the simulated data with fixed and incorrect parameter values. Usually, in least-squares analysis, the uncertainties in the parameters are estimated from the diagonal elements of the covariance matrix. However, the uncertainties from the diagonal elements do not include the effects of correlation between the parameters. For correlated parameters the actual uncertainties are larger than those from the covariance matrix [13,34]. In contrast, our technique of minimizing χ^2_R with one fixed parameter accounts for all correlations among the parameters because the parameters can vary to accommodate the incorrect value.

4.3. Analysis of three-component simulations

It is substantially more difficult to recover three decay times using either time-domain or frequency-domain data [17,35]. Additionally, with one exception [22], phase-modulation fluorometry at a single modulation frequency has not been used to determine more than two lifetimes. We reasoned that the availability of phase-sensitive intensities at multiple emission wavelengths would be adequate to resolve three-component mixtures. Hence, we investigated the resolution possible with the three-component mixtures simulated in fig. 2. The

dependence of χ^2_R on the three lifetimes is shown in fig. 6. The emission maxima of the three components are 330, 380 and 430 nm. The solid lines are data with $\tau_1 = 2.0$, $\tau_2 = 5.0$ and $\tau_3 = 8.0$ ns. The dashed lines are for the data with the same first and second lifetimes, but $\tau_3 = 3.5$ ns. The simulated data were analyzed from 330 and 430 nm, with 21 wavelengths, as shown by the two vertical dotted lines in fig. 2. The values of χ^2_R when τ_1 or τ_2 are varied are similar whether $\tau_3 = 3.5$ or 8.0 ns. Clearly, even for the three-component mixture, χ^2_R is highly sensitive to each of the three lifetimes. Of course, this sensitivity is somewhat less than for the two-component mixture, but the resolution must be regarded as adequate. The longest 8 ns lifetime shows the least resolution. However, even when τ_3 is held constant at 7.5 or 8.5 ns the increase in χ^2_R is still 2-fold. Hence, its lifetime is easily determined to ± 0.5 ns. If the data contain 4% noise the resolution of the lifetimes appears to be much less accurate (bottom, fig. 6). At 4% noise, resolution of the 5.0 ns lifetime is resolvable to ± 0.5 ns (if $\tau_2 = 4.5$ or 5.5 ns, $\chi^2_R = 1.5$) while that of the 8.0 ns lifetime appears resolvable within 1 ns (if $\tau_3 = 7$, 9 or 10 ns, $\chi^2_R = 1.5$, 1.2 or 1.9). The small changes in χ^2_R when the 8.0 ns lifetime is varied are mostly due to the amount of demodulation of the signal. When $\tau_3 = 3.5$ ns, at 1% noise the values of χ^2_R increase to 12 with a 0.5 ns shift and $\chi^2_R = 1.8$ at 4% noise. The relatively strong dependence of χ^2_R on the three lifetimes illustrates that even difficult three-component mixtures should be resolvable using our method.

The ability to determine the emission maxima of the three components remains good even for closely spaced lifetimes. This is illustrated in fig. 7. The solid lines again represent data with $\tau_3 = 8$ ns and the dashed lines data with $\tau_3 = 3.5$ ns. With

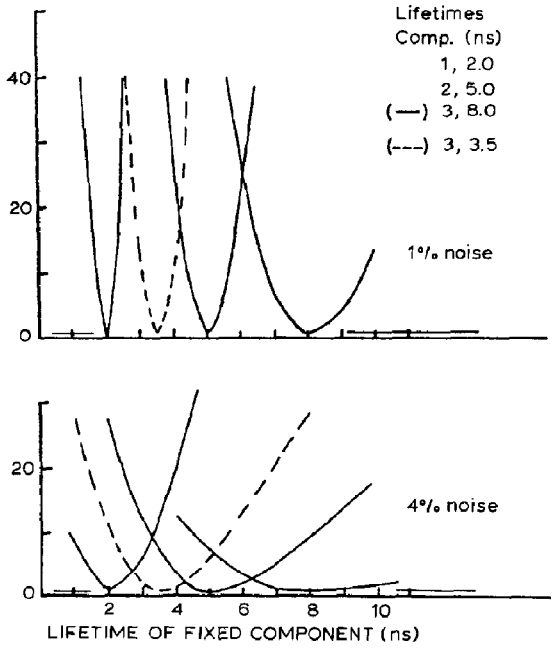

Fig. 6. The dependence of χ^2_R on the lifetimes of three-component mixtures. The simulated data (fig. 2) were fitted holding one lifetime constant at an incorrect value. $\tau_1 = 2$ (———), $\tau_2 = 5$ (———) and $\tau_3 = 8$ (———) or 3.5 ns (— — —); $\bar{\lambda}_1 = 330$ and $\bar{\lambda}_3 = 380$ and $\bar{\lambda}_3 = 430$ nm. Twenty simulated phase-sensitive spectra were analyzed representing the same values of ϕ_D as used in figs. 4–5.

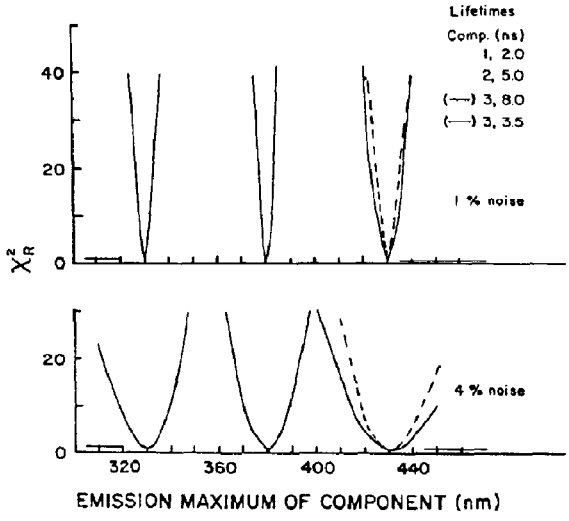

Fig. 7. The dependence of χ^2_R on the individual emission maxima for simulated three-component mixtures. The simulated data (fig. 6) were fitted using incorrect emission maxima for each component in turn, for data with $\tau_1 = 2$ (———), $\tau_2 = 5$ (———) and $\tau_3 = 8$ (———) or 3.5 ns (— — —). The correct emission maxima for the three components are 330, 380 and 430 nm, respectively.

1% noise the larger values of χ^2_R reveal 1–2 nm shifts from the correct emission maxima. Even at 4% noise, if $\tau_3 = 3.5$ or 8 ns, χ^2_R increases to 2-fold with a 5 nm shift in the third component spectrum. This increase is large enough to identify the shifted spectra as incorrect.

In fig. 3 we simulated a more difficult three-component sample with extensive overlap of the emission spectra. Even for this difficult case the phase-sensitive data provide reasonable resolution of the lifetimes (fig. 8) and emission maxima (fig. 9). While the sensitivity of χ^2_R is diminished as compared to the more widely spaced spectra, this dependence appears adequate to determine the correct lifetimes and emission maxima.

Frequently, phase-sensitive data can only be obtained in regions of strong spectral overlap. We simulated this restriction by using a smaller range of wavelengths, over which no single component contributes more than 90% of the emission for three-component data and 70% for the two-component data. These wavelength ranges are illustrated by the two vertical dashed lines in figs. 1–3. Reducing the wavelength range did not dramatically reduce the resolution of the two-component mixtures. This was also true for most of the three-component simulations when analyzed from 350 to 410 nm (fig. 2) or 330 and 390 nm (fig. 3), although at 4% noise the ability to resolve the lifetimes and emission maxima becomes very low. A decrease in the wavelength range is expected to result in the decreased resolution because a portion of the steady-state spectral shape is used in the fit. Of course, if the data do not include the emission maximum of a component, the ability to resolve its lifetime and fractional intensity decreases dramatically.

We note that the analysis of the simulated data shown cannot determine the precise resolution limits of this technique. The analysis of experimental data is complicated by additional factors, such as small fractional intensities and instrumental drift. However, the simulations do illustrate the appearance of phase-sensitive spectra and how the

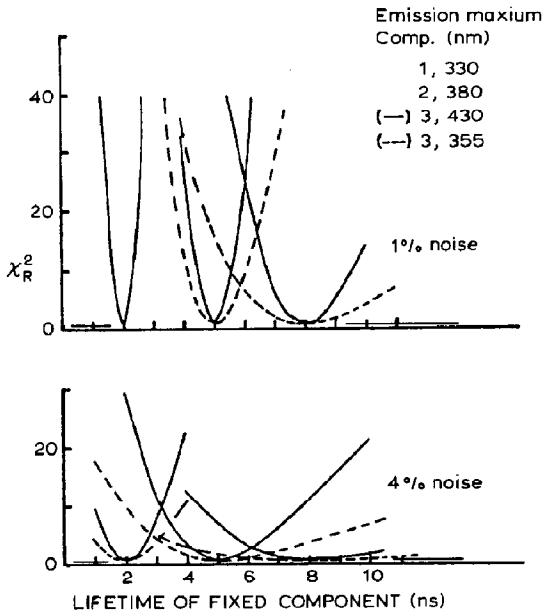

Fig. 8. The dependence of χ^2_R on the individual lifetimes for three strongly overlapping emission spectra. Fits of simulated data as in figs. 2 and 3. The correct lifetimes are 2, 5 and 8 ns. The emission maxima are 330, 380 and 430 nm (———) or 330, 380 and 355 nm (— — —). Other details are as for the data in fig. 6.

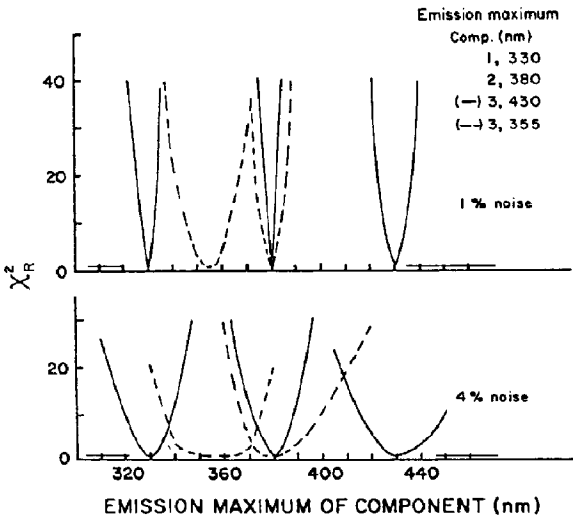

Fig. 9. The dependence of χ^2_R on the emission maxima of three strongly overlapping spectra. The correct emission maxima are 330, 380 and 430 nm (———) and 330, 380 and 355 nm (— — —). The correct lifetimes are 2, 5 and 8 ns.

lifetimes and steady-state spectra affect resolution of the components. As expected, more overlap of the steady-state spectra results in decreased precision in the resolution. Surprisingly, a decrease in the lifetime separation does not have a dramatic effect on the lifetime resolution. In fact, the lifetime resolution appears to be more affected by the modulation frequency and the extent of demodulation of each component. Lastly, large increases in χ^2_R result when incorrect spectra are used, demonstrating a strong dependence on the steady-state spectra given for each component.

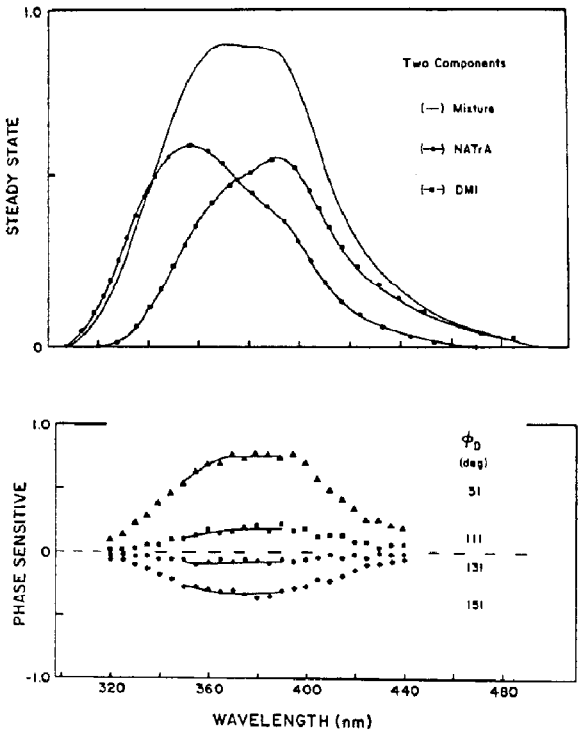

Fig. 10. A two-component mixture of NATrA and DMI. (Top) Steady-state emission spectra of NATrA (●———●) and DMI (■———■) at the same relative intensities as in the mixture (———). (Bottom) Phase-sensitive spectra of the mixture for $\phi_D = 31$, 111, 131 and 151°. All solutions were in 25 mM Tris-HCl (pH 7.5); 20°C. The solid lines indicate the calculated values and extend over the wavelength ranges used for analysis of the data.

4.4. Resolution of mixtures of indole, tyrosine and tryptophan derivatives

To demonstrate the usefulness of the technique in the study of protein fluorescence, we resolved two- and three-component mixtures of the tryptophan derivatives, NATrA, indole and DMI and the tyrosine derivative, NATyA. The steady-state spectrum of a two-component mixture of NATrA and DMI is shown in fig. 10 (———) with spectra of each component at the same concentration as in the two-component mixture. There is considerable overlap between these two spectra. The independently measured lifetimes are closely spaced at

Table 1

Resolution of NATrA and DMI mixtures

Spectra used in fit	Calculated		χ^2_R
	τ_i (ns)	f_i	
Solution A [a]			
NATrA	3.59	1.0	18.0
DMI	3.63	1.0	10.4
NATrA	2.95 [c] (0.02) [d]	0.41 (0.001) [d]	1.00
DMI	4.15 (0.02)	0.59 (0.001)	
NATrA	2.31	0.17	1.01
DMI	4.16	0.71	
Indole	4.04	0.12	
Solution B [b]			
NATrA	3.49	1.0	9.36
DMI	3.52	1.0	20.8
NATrA	3.07 (0.01)	0.59 (0.001)	1.01
DMI	4.26 (0.02)	0.41 (0.001)	
NATrA	3.01	0.46	1.68
DMI	4.51	0.58	
Indole	18.6	−0.04	

[a] The data were analyzed from 350 to 390 nm at 5-nm intervals (9 wavelengths) with an assumed noise level of 3%. Twelve files were used in the analysis, containing $12\phi_D$ between 0 and 220° for in-phase data and $12\phi_D$ between 90 and 310° for quadrature data. The steady-state fractional intensities of the components were approximately equal.

[b] As above but 20 files were used in the analysis (for in-phase data between 30 and 180°).

[c] The independently measured lifetime of NATrA is 2.92 (±0.18); DMI, 4.28 (±0.10) and indole, 4.47 (±0.17) ns.

[d] The values in parentheses are the standard deviations calculated from the diagonal values of the covariance matrix.

2.92 and 4.28 ns for NATrA and DMI, respectively (table 1). Representative phase-sensitive spectra of this mixture are shown in the lower panel of fig. 10. As the detector phase angle is increased from 31 to 151°, the phase-sensitive intensities decrease and become negative. Although the phase-sensitive spectral shape varies with detector phase angle, the separate contributions of the two components are not obvious for this sample. This is because the lifetimes are closely spaced and the spectra overlap strongly.

In least-squares analysis the number of components is usually estimated by varying the number of components to which the data are fitted. For example, for a two-component mixture, the phase-sensitive spectra can be fitted to a one-, two- or three-component decay. If the value of χ^2_R decreases significantly between the one- and two-component model then the sample is more accurately described by the two-component model (assuming the correct steady-state spectra are used in the analysis). Furthermore, if the value of χ^2_R does not decrease further when a third component is added, then the use of a third component is not justified [17].

Results from the least-squares analysis for the NATrA and DMI mixture are shown in table 1, for two separate but nearly identical mixtures (A and B). The steady-state fractional intensities of the two components are approximately equal in both mixtures. Data for wavelengths between 350 and 390 nm were analyzed. In this interval each component contributed to at least a third of the fluorescence intensity. When the data were fitted to a one-component model the resolved lifetime was intermediate between that of NATrA and DMI, but the values of χ^2_R ranged from 10 to 20. The individual values of χ^2_R depend on the steady-state spectra used in the one-component analysis. When fitted to a two-component model, using the steady-state spectra for NATrA and DMI, the value of χ^2_R decreased 14-fold to 1.0. When a third component was added to the analysis, in this case the steady-state spectrum of indole which is slightly blue-shifted from the NATrA spectrum (see fig. 11), the value of χ^2_R did not decrease. For the three-component fits, $\chi^2_R = 1.01$ and 1.68 for A and B respectively, and f_3 was small (0.12) or negative (−0.04). These results indicate that the two-component model is adequate to describe the data. Importantly, lifetimes recovered from the analysis (2.95 and 4.15 ns for A and 3.07 and 4.26 ns for B) agree with the independently measured lifetimes of NATrA and DMI of 2.92 (±0.18) and 4.28 (±0.10) ns, respectively. Furthermore, the recovered fractional intensities (f_i) from the two mixtures were 0.41 : 0.59 and 0.59 : 0.41, which agree with the expected values. The ability to recover the lifetimes and fractional intensities was only weakly dependent upon the number of wavelengths. For example, if the analysis of solution A was restricted to 7 wavelengths between 350 and 380 nm, the resolved lifetimes were 2.81 and 4.29 ns and $f_1 =$ 0.42. When the data for B were analyzed over 11 wavelengths between 350 and 400 nm, the resolved lifetimes were 3.04 and 4.33 ns and $f_1 =$ 0.56. These results demonstrate that phase-sensitive data can adequately resolve the lifetimes and fractional intensities of a two-component mixture with closely spaced spectra and with lifetimes that vary only 1.5-fold.

For a three-component sample we used a mixture of NATyA, NATrA and indole. The steady-state spectra are shown in fig. 11. The independently measured lifetime of NATyA was 1.51, NATrA, 2.92 and indole, 4.47 ns (table 2). This sample with a 3-fold range in lifetimes and the closely spaced spectra presents a difficult resolution as well as a model for the fluorescence of proteins containing tyrosine and tryptophan residues. Phase-sensitive spectra of this solution at four detector phase angles are shown at the bottom of the figure. The phase-sensitive intensities in the NATyA and NATrA regions of the spectra (on the short- and long-wavelength edges) become smaller at lower ϕ_D than the middle region containing the indole emission with its longer lifetime.

The results of the analysis are shown in table 2, along with those from a second similar sample. For both samples the steady-state fractional intensities were approximately equal. The data were analyzed using either 15 or 12 wavelengths between 310 and 380 nm. Two components each contribute at least 20% each of the total fluorescence over this wavelength range. We note that by

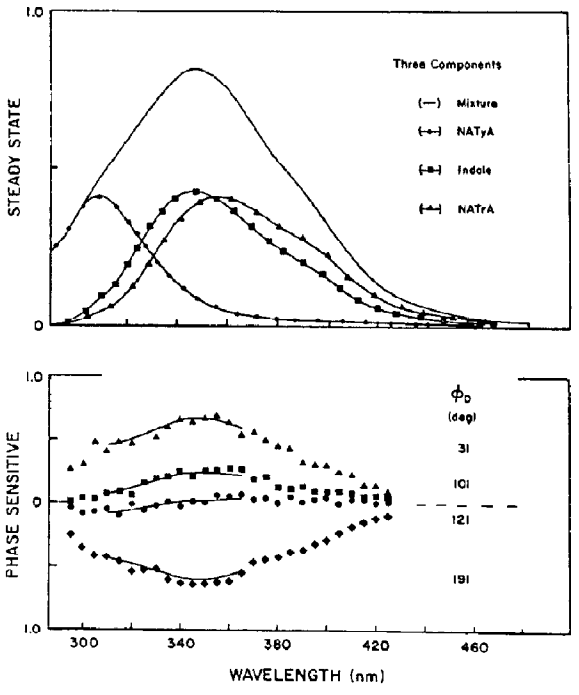

Fig. 11. Three-component mixture of NATrA, NATyA and indole. (Top) Steady-state emission spectra of NATyA (●———●), indole (■———■), and NATrA (▲———▲) at the same relative intensities as in the mixture (———). (Bottom) Phase-sensitive spectra for $\phi_D = 31$, 101, 121 and 191°. Other conditions as in fig. 10.

restricting the wavelengths to the region of strong overlap we increased the difficulty of the resolution. If all the available wavelengths were used we would have had data for wavelengths for which the emission was dominated by a single fluorophore. This would determine the lifetime of this component (i.e., decrease correlation between the parameters) and stabilize the solution.

When the data from the three-component mixture were fitted using any two of the three-component spectra the value of χ^2_R ranged from 2 to 33. However, when the data were fitted to a three-component model, the values of χ^2_R dropped 15-fold to 0.866 for A and 2.9-fold to 1.36 for B. When the data were fitted to a four-component model using a DMI spectrum as the fourth component, the values of χ^2_R were large and unreproducible. In addition, f_2 was negative in both cases. Therefore, the three-component model appears to give the best fit to the data. The lifetimes recovered from the analysis were within the day-to-day error in the independently measured values of NATyA, NATrA and indole (table 2) of 1.51

Table 2

Resolution of NATyA, NATrA and indole mixtures [a]

Spectra used in fit	Calculated τ_i (ns)	f_i	χ^2_R
Solution A [b]			
NATyA	1.79	0.32	2.57
NATrA	3.59	0.68	
NATyA	1.12	0.22	3.06
Indole	3.61	0.76	
NATrA	0.663	−0.61	32.6
Indole	2.02	1.61	
NATyA	1.41 [d] (0.01)	0.27 (0.001)	0.866
NATrA	2.84 (0.03)	0.33 (0.001)	
Indole	4.62 (0.03)	0.40 (0.001)	
NATyA	3.10	0.53	2004
NATrA	1.82	−5.4	
Indole	2.12	2.6	
DMI	1.71	3.3	
Solution B [c]			
NATyA	1.79	0.31	1.78
NATrA	3.56	0.69	
NATyA	1.06	0.20	1.78
Indole	3.57	0.80	
NATrA	0.633	−0.62	8.13
Indole	1.99	1.62	
NATyA	1.39 (0.02)	0.25 (0.001)	1.36
NATrA	2.89 (0.08)	0.34 (0.002)	
Indole	4.42 (0.08)	0.41 (0.004)	
NATyA	−0.881	0.21	207
NATrA	3.06	−5.4	
Indole	3.49	4.1	
DMI	3.00	2.1	

[a] Analysis of data as in table 1 except where indicated.

[b] Data from 14 files (in-phase data between 0 and 260°) were fitted using an assumed noise level of 2.5%, between 310 and 380 nm (15 wavelengths).

[c] Data from 20 files (in-phase data between 20 and 180°) were analyzed using an assumed noise level of 4%, between 310 and 365 nm (12 wavelengths).

[d] The independently measured lifetime of NATyA is 1.51 (±0.19); NATrA, 2.92 (±0.18); indole, 4.47 (±0.17) and DMI, 4.28 (±0.10) ns.

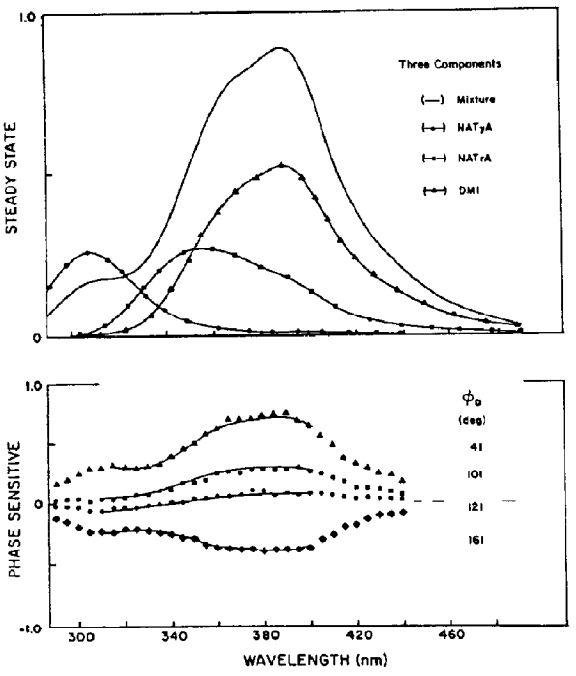

Fig. 12. Three-component mixture of NATyA, NATrA and DMI. (Top) Steady-state emission spectra of NATyA (●———●), NATrA (■———■) and DMI (▲———▲) at the same relative intensities as in the mixture (———). (Bottom) Phase-sensitive spectra at $\phi_D = 41$, 101, 121 and 161°. Other conditions as in fig. 10.

(±0.20), 2.92 (±0.18) and 4.47 (±0.17) ns. For A the lifetime values were 1.41, 2.84 and 4.62 ns and for B, 1.39, 2.89 and 4.42 ns. In addition, the resolved fractional intensities were close to the equal ratios expected for both solutions A and B: 0.27 : 0.33 : 0.40 and 0.25 : 0.34 : 0.41. When the data from solution B were analyzed over 15 wavelengths (310–380 nm) as for A, the results were similar, $\tau_1 = 1.38$, $\tau_2 = 2.81$ and $\tau_3 = 4.59$ ns while $f_1 = 0.22$ and $f_2 = 0.38$. The successful analysis of this mixture demonstrates that this nonlinear least-squares analysis can be used to determine the component lifetimes and fractional intensities for three-component solutions, in the ultraviolet region, with closely spaced lifetimes and considerable spectral overlap. It should be noted that the solution B data are our poorest data set, with 4% noise, but the lifetimes are still resolvable.

We also examined three-component mixtures of NATyA, NATrA and DMI. In this case mixture A contained the three components at equal steady-state intensities, while in solution B the intensities of NATyA and NATrA were approximately equal and DMI was present at twice the steady-state intensity of the other fluorophores (fig. 12, top).

Table 3

Resolutions of NATyA, NATrA and DMI mixtures [a]

Spectra used in fit	Calculated		χ^2_R
	τ_i (ns)	f_i	
Solution A [b]			
NATyA	1.28	0.31	9.68
NATrA	3.45	0.69	
NATyA	1.78	0.44	9.29
DMI	3.51	0.56	
NATrA	2.07	1.19	82.4
DMI	−2.96	−0.19)	
NATyA	1.61 [d] (0.01)	0.36 (0.001)	1.07
NATrA	2.90 (0.02)	0.34 (0.001)	
DMI	4.10 (0.02)	0.30 (0.001)	
NATyA	−0.776	0.081	197
NATrA	670000	0.0	
DMI	5.85	0.23	
Indole	10.1	0.69	
Solution B [d]			
NATyA	−0.757	0.08	39.7
NATrA	3.71	0.92	
NATyA	1.87	0.20	8.23
DMI	3.78	0.80	
NATrA	2.25	0.49	19.8
DMI	5.55	0.51	
NATyA	1.58 (0.01)	0.15 (0.001)	0.892
NATrA	2.85 (0.01)	0.27 (0.001)	
DMI	4.19 (0.01)	0.58 (0.001)	

[a] Analysis of data as in table 1 except where indicated.

[b] Data from 14 files (in-phase data between 0 and 260°) were analyzed using an assumed noise level of 3%, between 310 and 390 nm (17 wavelengths).

[c] Data from 20 files (in-phase between 30 and 180°) were fitted using an assumed noise level of 2.5%, between 310 and 400 nm (19 wavelengths). The steady-state fractional intensity of DMI was approximately twice that of NATyA and NATrA.

[d] The independently measured lifetime of NATyA is 1.51 (±0.19); NATrA, 2.92 (±0.18); DMI, 4.28 (±0.10) and indole, 4.47 (±0.17) ns.

The independently measured lifetimes of the three components vary over a 2.8-fold range (table 3). In the phase-sensitive spectra (fig. 12, bottom) the contributions from NATyA and NATrA at shorter wavelengths become small and negative before the longer-lived DMI signal at about 380 nm. The data were analyzed at 17 or 19 wavelengths between 310 and 400 nm (table 3). When the data were fitted to a three- rather than a two-component model the value of χ^2_R decreased about 28-fold to 1.07 and 0.892 for A and B. As for the previous three-component mixture (table 2), when a fourth component was added to the analysis, such as an indole spectrum, χ^2_R increased and one of the calculated fractional intensities was zero. Importantly, the fractional intensities from the three-component fit were as expected. For the first mixture the steady-state fractional intensities were approximately equal (spectra not shown): 0.36 : 0.34 : 0.30. For B, as expected from fig. 12, the intensity of DMI is about twice that of NATyA and NATrA: 0.15 : 0.27 : 0.58. The lifetimes are also close to the independently measured values: for NATyA, 1.61 and 1.58 ns; for NATrA, 2.90 and 2.85 ns and for DMI, 4.10 and 4.19 ns. These results show that this technique can be used to resolve successfully the lifetimes and fractional intensities from a three-component mixture even when more than half the steady-state intensity is due to one component.

5. Conclusions

The successful resolution of the two- and three-component mixtures demonstrates the usefulness of phase-sensitive detection for the analysis of multi-component mixtures, including the tyrosine and tryptophan fluorescence from proteins. We found that correct lifetimes and fractional intensities could be obtained from fits of phase-sensitive data over wavelengths where all components contributed to the emission. Furthermore, previous knowledge of either the fractional intensities or lifetimes was not required or used for the resolutions. However, it is necessary to know or to assume the spectral shape of each component used in the analysis. This is clearly an improvement over previous resolutions of two-component phase modulation data from fixed frequency instruments, using analytical and fitting methods, where the input of the apparent phase and modulation lifetime data from more than one frequency is generally required [9,10,12–14]. This method is also an improvement on that used by McGown and Bright [23–25] where the phase-sensitive intensities of the individual components must be measured at each detector phase angle. Our method does not require separate phase-sensitive data for each component, but relies instead on the well known dependence of the phase-sensitive spectra on the fluorescence lifetimes. The phase angle, or lifetime, of each component is determined from the phase-sensitive intensities of the individual components. These wavelength-independent lifetimes serve in the determination of the contributions of each component. In some respects this method is analogous to the global methods described by Beechem and co-workers [13,36,37] in that the lifetimes are variable parameters, but are constrained to be constant across the emission spectrum of each component. This linkage is probably an essential stabilizing feature of our method of analysis.

A clear disadvantage of this technique is the requirement for known steady-state spectra. Yet this is not quite as limiting a factor as it may appear. For a two-component sample, one or two of the component spectra are often known. For instance, for a tryptophan-containing protein, the spectrum of an exposed residue can be determined from quenching experiments [8,38]. Alternatively, a model tryptophan spectrum can be recorded and the spectrum moved along the emission wavelength axis to generate several spectra with different emission maxima. The phase-sensitive data can be fitted using the spectra from the quenching experiments and/or the model spectra. Analysis of the data can be performed using different model spectra until a set of spectra is found which explains the data.

Finally, the restriction of known emission spectra can be eliminated when phase-sensitive spectra are recorded at multiple modulation frequencies. Frequency-domain fluorometers using the essential cross-correlation technique have now been

constructed in at least two laboratories [26,27]. These instruments considerably extended the resolving power of phase modulation fluorescence spectroscopy. Such instruments permit the resolution of multi-exponential emission from data recorded at many frequencies, without previous knowledge of the lifetimes, fractional intensities or steady-state spectra of the components [17,27–29]. The use of phase-sensitive detection at multiple modulation frequencies should allow resolution of both the lifetimes and emission spectra of multi-component solutions, perhaps containing four or five emitting species. This extension of phase-sensitive detection to multi-frequency data is currently in progress.

Acknowledgements

The authors acknowledge the support of the National Science Foundation, Biophysics and Biological Instrumentation Programs (PCM 82-10878, 81-06910, DBM-8502835 and DBM-8511065). H.C. expresses appreciation for financial support from Research Project CPBP01.06 (Poland). We thank Dr. Gabor Laczko for his assistance in interfacing the computer to the phase fluorometer. H.C. is on leave from Nicholas-Copernicus University, Torun, Poland.

References

1 M.G. Badea and L. Brand, Methods Enzymol. 61 (1979) 378.
2 J.R. Knutson, J.M. Beechem and L. Brand, Chem. Phys. Lett. 102 (1983) 501.
3 I. Isenberg, Biophys. J. 43 (1983) 141.
4 L.J. Libertini and E.W. Small, Anal. Biochem. 138 (1984) 314.
5 D.V. O'Connor and D. Phillips, Time-correlated single photon counting (Academic Press, New York, 1984).
6 T. Lin and R.M. Dowben, in: Excited states of biopolymers, ed. R.F. Steiner (Plenum Press, New York, 1983).
7 J.N. Demas, Excited state lifetime measurements (Academic Press, New York, 1983).
8 J.R. Lakowicz, Principles of fluorescence spectroscopy (Plenum Press, New York, 1983).
9 G. Weber, J. Phys. Chem. 85 (1981) 949.
10 D.M. Jameson and G. Weber, J. Phys. Chem. 85 (1981) 953.
11 M.R. Eftink and D.M. Jameson, Biochemistry 21 (1982) 4443.
12 D.M. Jameson and E. Gratton, in: New directions in molecular luminescence, ed. P. Eastwood (American Society for Testing and Materials, 1983) p. 67.
13 J.M. Beechem, J.R. Knutson, J.B.A. Ross, B.W. Turner and L. Brand, Biochemistry 22 (1983) 6054.
14 R.E. Dalbey, J. Weiel, W. Perkins and R.G. Yount, J. Biochem. Biophys. Methods 9 (1984) 251.
15 T.V. Veselova, A.S. Cherkasov and V.I. Shirokov, Opt. Spectrosc. 29 (1970) 617.
16 J.R. Lakowicz and H. Cherek, J. Biochem. Biophys. Methods 5 (1981) 19.
17 J.R. Lakowicz, G. Laczko, H. Cherek, E. Gratton and M. Limkeman, Biophys. J. 46 (1984) 463.
18 J.R. Lakowicz and H. Cherek, J. Biol. Chem. 256 (1981) 6348.
19 J.R. Lakowicz and A. Balter, Photochem. Photobiol. 36 (1982) 125.
20 J.R. Lakowicz and S. Keating, J. Biol. Chem. 258 (1983) 5519.
21 J.R. Lakowicz, R.B. Thompson and H. Cherek, Biochim. Biophys. Acta 734 (1983) 295.
22 S. Keating-Nakamoto, H. Cherek and J.R. Lakowicz, Anal. Biochem. 148 (1985) 349.
23 L.B. McGown and W.V. Bright, Anal. Chem. 56 (1984) 1400.
24 L.B. McGown, Anal. Chim. Acta 157 (1984) 327.
25 L.B. McGown and E.V. Bright, Anal. Chem. 56 (1984) 2198.
26 E. Gratton and M. Limkeman, Biophys. J. 44 (1983) 315.
27 J.R. Lakowicz and B.P. Maliwal, Biophys. J. 21 (1985) 61.
28 E. Gratton, M. Limkeman, J.R. Lakowicz, B. Maliwal, H. Cherek and G. Laczko, Biophys. J. 46 (1984) 479.
29 J.R. Lakowicz, E. Gratton, H. Cherek, B.P. Maliwal and G. Laczko, J. Biol. Chem. 259 (1984) 10967.
30 R.D. Spencer and G. Weber, Ann. N.Y. Acad. Sci. 158 (1969) 361.
31 P.R. Bevington, Data reduction and error analysis for the physical sciences (McGraw-Hill, New York, 1969).
32 R.W. Engstrom, Photomultiplier handbook (RCA Corporation, Lancaster, PA, 1980).
33 J.R. Lakowicz, H. Cherek and A. Balter, J. Biochem. Biophys. Methods 5 (1981) 131.
34 J. Johnson, Biophys. J. 44 (1983) 101.
35 A. Grinvald and J.Z. Steinberg, Anal. Biochem. 59 (1974) 583.
36 J.M. Beechem, M. Ameloot and L. Brand, Chem. Phys. Lett. 120 (1985) 466.
37 J.R. Knutson, J.M. Beechem and L. Brand, Chem. Phys. Lett. 102 (1983) 501.
38 S.S. Lehrer, Biochemistry 10 (1971) 3254.